D N 4, 2007
Preprint typeset using LaTeX style emulateapj v. 05/04/06

OFF-CENTER IGNITION IN TYPE IA SUPERNOVA: I. INITIAL EVOLUTION AND IMPLICATIONS FOR DELAYED DETONATION

F. K. R¨ [1,2], S. E. W [1] W. H [2]

Draft version November 4, 2007

ABSTRACT

The explosion of a carbon-oxygen white dwarf as a Type Ia supernova is known to be sensitive to the manner in which the burning is ignited. Studies of the pre-supernova evolution suggest asymmetric, off-center ignition, and here we explore its consequences in two- and three-dimensional simulations. Compared with centrally ignited models, one-sided ignitions initially burn less and release less energy. For the distributions of ignition points studied, ignition within two hemispheres typically leads to the unbinding of the white dwarf, while ignition within a small fraction of one hemisphere does not. We also examine the spreading of the blast over the surface of the white dwarf that occurs as the first plumes of burning erupt from the star. In particular, our studies test whether the collision of strong compressional waves can trigger a detonation on the far side of the star as has been suggested by Plewa et al. (2004). The maximum temperature reached in these collisions is sensitive to how much burning and expansion has already gone on, and to the dimensionality of the calculation. Though detonations are sometimes observed in 2D models, none ever happens in the corresponding 3D calculations. Collisions between the expansion fronts of multiple bubbles also seem, in the usual case, unable to ignite a detonation. "Gravitationally confined detonation" is therefore not a robust mechanism for the explosion. Detonation may still be possible in these models however, either following a pulsation or by spontaneous detonation if the turbulent energy is high enough.

Subject headings: Stars: supernovae: general — hydrodynamics – instabilities — turbulence — methods: numerical

1. INTRODUCTION

In the currently favored model for Type Ia supernovae (SNe Ia), a carbon-oxygen white dwarf (WD) grows to almost the Chandrasekhar mass, then explodes due to a thermonuclear instability (e.g., Hillebrandt & Niemeyer 2000). While the modeling of the explosion itself has reached a high level of sophistication, with multi-dimensional studies being routinely carried out by several groups (e.g. Reinecke et al. 2002b; Gamezo et al. 2003; Plewa et al. 2004; Röpke & Hillebrandt 2004, 2005a; García-Senz & Bravo 2005; Röpke et al. 2006a), the initial conditions of this process remain largely unknown. This is unfortunate since the geometry of the flame ignition has a large effect on the explosion strength (Niemeyer et al. 1996; Livne et al. 2005; Röpke et al. 2006b; Schmidt & Niemeyer 2006).

Runaway commences once the WD has accreted sufficient matter from a binary companion to approach a central density $\sim 3 \times 10^9$ g cm^{-3} where plasma neutrino losses are exceeded by energy generation from a highly screened carbon fusion reaction. The stage for flame ignition is set by a century of convective carbon burning in the progenitor WD. It remains unclear, however, if the first sparks to develop a nearly discontinuous temperature gradient on their perimeters (the "flame") are concentrated in the center of the star (Höflich & Stein 2002) or spread around by the convective flow in which they are embedded. Since this convective flow may have a dipole character, one natural possibility is lopsided ignition displaced somewhat off-center (e.g., Woosley et al. 2004).

It is known that, once born, the flame experiences an extended period of subsonic propagation—a "deflagration" (Nomoto et al. 1976). Prompt detonation is excluded on the grounds that it would produce spectroscopy, nucleosynthesis, and a light curve very different from observations (see Filippenko 1997, for a review). It would also require a degree of isothermality in the core that would be very difficult to achieve (Woosley 1990). The deflagration poses a computational challenge since the ashes of the burning are buoyant, and that leads to instabilities and turbulence that can only be followed with any accuracy in a multi-dimensional calculation. The difficulty is compounded by the large range of spatial scales—sub-millimeter for the flame width and Kolmogorov scale to 2,000 km for the WD—and the high Reynolds number, $Re \sim 10^{14}$.

Calculations of the same WD differ in outcome because of the assumptions about ignition, various techniques used to treat flame instabilities, and turbulence. It is not practical to resolve both the flame and the star, so full-star models, such as the ones presented here, rely upon an effective flame model and a subgrid scale model for the turbulence. Qualitatively, the flame advances radially at a speed given by the flotation of the largest plumes, but the lateral spreading of each plume and the overall efficiency of the explosion can vary, depending upon the way turbulence is handled, and on the dimensionality and resolution of the model. Results of different approaches have been published in a variety of studies with the general conclusion that a pure deflagration can give a viable explosion (Reinecke et al. 2002b; Gamezo et al. 2003; Röpke & Hillebrandt 2005a), not too different from what is observed (Travaglio et al. 2004; Blinnikov et al. 2006). It remains controversial, however, if these models can give light curves as bright as some observations indicate, or can explain all of the spectroscopic features (Gamezo et al. 2003; Kozma et al. 2005).

Moreover, these successful models all have in common the assumption of nearly isotropic central ignition. It may be

[1] Department of Astronomy and Astrophysics, University of California, Santa Cruz, CA 95064, U.S.A.
[2] Max-Planck-Institut für Astrophysik, Karl-Schwarzschild-Str. 1, D-85741 Garching, Germany

that nature provides only anisotropic ignition conditions, or it may be that the the observational constraints on a pure deflagration will ultimately prove too stringent. In these cases, a transition to detonation may need to occur (Plewa et al. 2004; Livne et al. 2005). The idea of a delayed detonation has been around for some time (Khokhlov 1991; Woosley & Weaver 1994), but the physics of that transition, if it happens, is still uncertain (Niemeyer & Woosley 1997; Niemeyer 1999). Recent two-dimensional calculations have suggested that burned material may quickly ascend to the surface of the still gravitationally bound star, sweep around it and, by collision and compression on the opposite side, trigger a detonation in the unburned material (Plewa et al. 2004). This is called by its proponents "gravitationally confined detonation", or GCD.

Here, we follow the evolution of one-sided ignitions for a range of assumptions regarding the initial conditions in two-dimensional (2D) and three-dimensional (3D) simulations. The results are sensitive to the fuel consumption and energy release during the rising stage of the plume. Therefore a correct description of the turbulent deflagration flame is as crucial here as in other models. We describe our approach in Sect. 3. Before that, we give a brief motivation of the ignition scenarios explored here. Although Röpke et al. (2006b) showed that ignition conditions cannot be explored reliably in 2D simulations, we can and do use surveys in cylindrical symmetry to get a feeling for the parameter range to be explored, as well as the dependence of the results on numerical resolution (Sect. 4). Full-star 3D simulations are presented in Sect. 5, and the consequences regarding the possibility of triggering a detonation are discussed in Sect. 6. Conclusions are drawn in Sect. 7.

2. OFF-CENTER IGNITION

Several studies now suggest ignition with an offset from the center of the WD of order $100 \ldots 200$ km (Garcia-Senz & Woosley 1995; Woosley et al. 2004; Wunsch & Woosley 2004; Kuhlen et al. 2006; Iapichino et al. 2006). It should be acknowledged that none of these studies has yet followed the actual transition from a high temperature fluctuation to a flame in a self-consistent way, including the possibility the perturbation is disrupted by turbulence, and all fall far short of the actual Reynolds number in the star. Also, while arguments based upon a probability density function can offer some guidance as to whether a particular temperature is likely to be realized, they cannot, by themselves, say whether the high temperature happens in a contiguous region, or in many disparate points, or even over some interval of time.

Still, the calculations of Kuhlen et al. (2006) do suggest that ignition is unlikely to occur as a single spherical bubble either at the center or off-center. Rather the distribution of high temperature may look more like a "teardrop", spreading as it goes out to a large opening angle. We thus explore here a variety of initial conditions ranging from nearly spherical bubbles far off center, to ignition in multiple points forming complex configurations. The models are named according to their dimensionality and the ignition characteristics where "B" stands for a single bubble (spherical as much as Cartesian coordinates allow) with an attached number indicating its radius in kilometers, "P" is a highly perturbed bubble,"T" stands for a teardrop distribution of multiple bubbles followed by a "1" to indicate a strictly one-sided ignition and by a "2" when the ignition region overshoots to the opposite side. Where appropriate, "d" followed by a number gives the distance of the ignition center from the middle of the WD in the bubble case (and the maximum extent of ignition measured from the WD's center in the teardrop case). For example, Model 3B50d200 is a 3D simulation with an ignition in form of a spherical bubble of radius 50 km centered 200 km from the middle of the star. There may also be variations on these names based upon resolution (a,b,c, etc).

3. THE ASTROPHYSICAL AND NUMERICAL MODEL

The implementation of the deflagration SN Ia model follows the detailed descriptions given by Reinecke et al. (1999, 2002a); Röpke (2005) and Schmidt et al. (2006b). The hydrodynamics is modeled via the piecewise parabolic method (Colella & Woodward 1984) in the P implementation (Fryxell et al. 1989), in combination with a WD matter equation of state incorporating an electron gas relativistic and degenerate to variable degrees, a Boltzmann gas of nuclei, photons and electron-positron pairs.

Since the results are sensitive to small perturbations of the initial flame configuration, the directional splitting in the hydrodynamics solver, as well as discretization errors on the Cartesian grid may provide seeds for developing instabilities. This is not necessarily unphysical. In a realistic SN Ia explosion, the background is not expected to be smooth, nor will the initial flame shape be perfectly regular. But, as discussed below, one sometimes has little control over these effects.

Another crucial aspect of the modeling is the prescription for flame propagation. We strive to implement here a consistent model for burning in the flamelet regime following standard theories of turbulent combustion—such as they are. The fundamental assumption is the establishment of a turbulent cascade from large-scale eddies produced by shear instabilities at the interfaces of burning bubbles down to the Kolmogorov scale, where viscous effects dissipate the turbulent kinetic energy. The flame interacts with turbulence down to the Gibson scale, where the laminar burning speed s_l becomes comparable to the turbulent velocity fluctuations v'. By definition in the flamelet regime, this Gibson scale is large compared to the width of the flame—a condition that holds for most parts of the supernova explosion until quite low densities are reached (for an approach to modeling stages beyond this regime see Röpke & Hillebrandt 2005b). Thus the internal flame structure remains unaffected by turbulent eddies. Damköhler (1940) first pointed out that the turbulent flame front in these circumstances should propagate with an effective velocity that is proportional to the turbulent velocity fluctuations and independent of the burning microphysics.

Following this concept, the flame is modeled as a sharp interface separating the fuel from the ashes. Its propagation is followed in a level set approach (Osher & Sethian 1988), where the flame front is associated with the zero level set of a scalar, G, defined to be a signed distance function away from the flame. This front is advanced as described by Reinecke et al. (1999).

The speed of flame propagation is a function of the turbulent velocity fluctuations on the scale of the computational grid cells. Its value is determined from a subgrid-scale turbulence model. In the 2D simulations, this model is implemented according to Niemeyer & Hillebrandt (1995), and the turbulent flame speed, s_t, is set equal to the turbulent velocity fluctuations, $v' = \sqrt{2k_{\rm sgs}}$, where $k_{\rm sgs}$ denotes the subgrid-scale turbulent specific kinetic energy. The 3D simulations employ an improved subgrid-scale model (Schmidt et al. 2006a,b). That model, based upon localized closures for the terms of

the balance equation of turbulent subgrid-scale energy, does not need to assume a specific scaling behavior of the turbulent cascade, nor isotropy of the turbulence. The flame propagation speed is implemented as

$$s_{\rm t} = s_{\rm l}\sqrt{1 + C_{\rm t}\left(\frac{q_{\rm sgs}}{s_{\rm l}}\right)^2}$$

with $C_{\rm t} = 4/3$ and $q_{\rm sgs}$ denoting the subgrid-scale turbulence velocity (Pocheau 1994; Schmidt et al. 2006b).

Nuclear reactions are implemented in a simple way described by Reinecke et al. (2002a). Only four species, ^{12}C, ^{16}O, ^{24}Mg, ^{56}Ni, and α-particles, are taken into account. Material traversed by the flame front is converted to a composition represented by a temperature-dependent mixture of ^{56}Ni and α-particles in nuclear statistical equilibrium, or, at fuel densities below $5.25 \times 10^7\,{\rm g\,cm^{-3}}$, to intermediate mass elements represented by ^{24}Mg. At fuel densities below $10^7\,{\rm g\,cm^{-3}}$ nuclear reactions are assumed to cease.

In all simulations the WD was set up cold and isothermal with a temperature of $T = 5 \times 10^5\,{\rm K}$ and a central density of $\rho_{\rm c} = 2.9 \times 10^9\,{\rm g\,cm^{-3}}$ composed of equal parts of carbon and oxygen.

The discretization on the computational grid follows the strategy of two nested moving grids suggested by Röpke et al. (2006b), where a fine-resolved uniform inner grid contains the flame while an outer grid with exponentially growing grid cells accommodates the WD star and follows its expansion. Due to flame propagation inside the WD, it is possible to subsequently collect adjacent grid cells of the outer grid into the uniform part, as soon as the cell sizes match thereby optimizing the resolution for the given number of computational grid cells.

4. EXPLORING THE POSSIBILITIES: 2D SIMULATIONS

The parameter space and the dependence of the results on numerical resolution were first explored assuming cylindrical symmetry. The results obtained in 2D should not be used to draw quantitative conclusions, but are a numerically inexpensive way to explore a broad range of possibilities.

In the cylindrical (r, z)-setups, the entire WD was accommodated on the grid, from its center to its radius assuming rotational symmetry about the z-axis (see top left panel of Fig. 1).

4.1. *Single-bubble ignition*

As a first numerical experiment, the flame was initiated in the simplest conceivable configuration: a single spherical bubble ignited somewhere on the z-axis. Even this simple configuration has three parameters that potentially impact the evolution of the explosion. One is the resolution of the flame and the WD star. Two additional parameters—the displacement of the igniting bubble from the center of the WD and its radius—are more physical in nature. As an illustrative model, consider one where ignition took place 200 km off-center in a spherical bubble of radius 50 km (cf. Fig. 1). The resolution for this example study (Model 2B50d200c, Table 1) was 256 grid cells in r-direction and 512 grid cells in z-direction, and the initial setup is shown in the top left panel of Fig. 1. In the top middle panel, a close-up on the flame illustrates the evolution from the initial spherical shape to a more irregular toroidal structure. This is a consequence of the buoyancy-induced flotation of the bubble acting in combination with self-propagation of the flame due to burning. The flame floats towards the surface of the star, thereby being subject to considerable lateral spread (cf. snapshots at $t = 0.5\,{\rm s}$ and $t = 1.0\,{\rm s}$ in Fig. 1). At $t \sim 2\,{\rm s}$, burning has ceased since the fuel density ahead of the flame has dropped below $10^7\,{\rm g\,cm^{-3}}$. The burned material sweeps around the star since it is still gravitationally bound. Although it extends to rather large radii, only about $0.49\,M_\odot$ is located outside a radius of $2.5 \times 10^8\,{\rm cm}$ at $t = 2\,{\rm s}$. Only $\sim 0.1\,M_\odot$ of the WD is burned, inadequate to unbind the star. In the outer layers of the WD opposite to the flame ignition, burned material collides subsonically with a compressional front moving ahead of the actual ash. In the simulation, the evolution continues by an expansion of the outer layers while the central parts of the WD contract such that the inner parts of the flame eventually reach fuel densities above the threshold of $10^7\,{\rm g\,cm^{-3}}$. In our flame description burning resumes at this point, and the newly processed material is expelled into the ash region (cf. Fig. 1, snapshot at $t = 6.0\,{\rm s}$). This, however, is sensitive to the way burning is implemented in the code (either completely "on" for densities above 10^7 g cm^{-3}, or "off" for lower densities) and may not be a realistic occurrence.

As pointed out by Plewa et al. (2004), the collision of the gravitationally bound material sweeping around the surface of the WD marks an interesting point in the evolution. To initiate a spontaneous detonation, high density and temperature are both necessary in the unburned material at the focus of the collision. The cylindrical-symmetric setup forces the collision of burned material to take place at the negative part of the z-axis. Figure 2 shows the temperature of the material in the model described above. The snapshot was taken at the instant of peak temperature in the compressed fuel in the collision region. The peak temperature there was $2.22 \times 10^9\,{\rm K}$ at a density of $1.41 \times 10^6\,{\rm g\,cm^{-3}}$. As will be discussed, the conditions reached in the collision depend on the parameters of the setup as discussed.

4.1.1. *A note on numerical convergence*

Two sets of simulations with spherical initial flames were carried out varying the number of cells in the computational grid. One had an initial bubble radius of 50 km, and the other, a bubble radius of 25 km. For each simulation, the maximum temperature in the unburned material in the collision region was determined, along with the nuclear energy release prior to reaching this temperature. The results are given in Table 1. There is significant scatter in the critical collision temperature with values deviating by up to 43%. A similar variation is seen in the energy of the burning. Although a clear trend is not apparent in Table 1, it seems that better numerical resolution leads to less energy release in the burning, less expansion, and hence to a stronger collision in the unburned material. The scatter is larger when starting with bubbles of smaller radius.

Previous studies suggest convergent results should be obtained with a resolution of about 256 cells per dimension in one octant (Reinecke et al. 2002a; Röpke 2005). Here the situation is different. While previous resolution studies were carried out on the basis of an initial flame setup with well specified perturbations imposed on it, all seeds for growing nonlinear instabilities in the spherical bubble setup applied here are introduced by numerical artifacts, such as discretization errors and noise. This setup is not a well-posed numerical problem because the evolution of nonlinear features in the flame structure is expected to be strongly resolution dependent and thus numerical convergence is problematic. Given that the flame evolution is dominated by strongly nonlinear

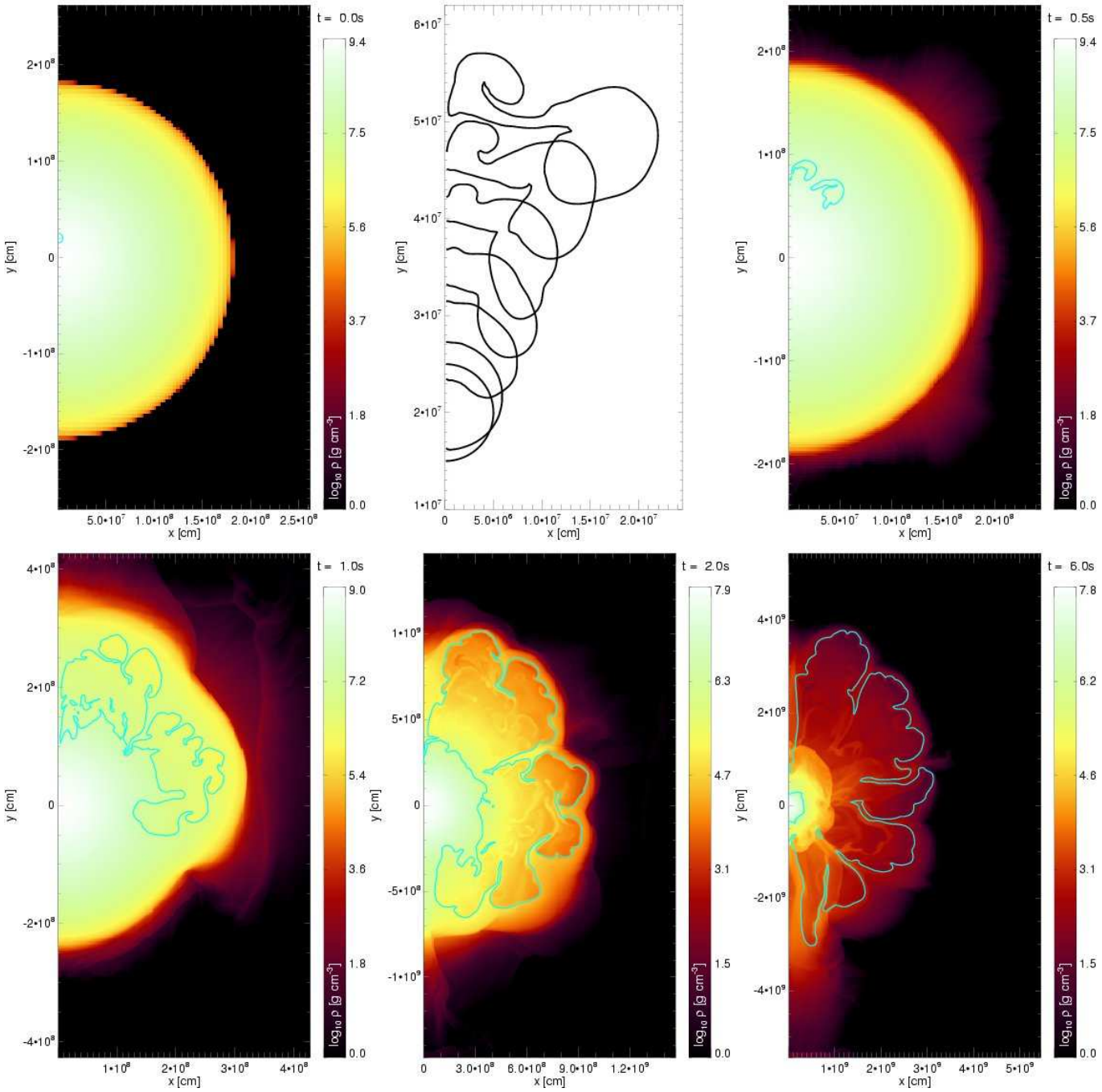

F . 1.— Evolution of a 2D explosion simulation (Model 2B50d200c) ignited in a single bubble 200 km off-center. The top-middle panel illustrates the flame front evolution in the interval $t = [0, 0.3]$ s. Each contour corresponds to a time step of 0.05 s. In all other snapshots, the cyan isosurface corresponds to the zero level set of G which is associated to the flame front in early stages of the evolution and indicates the interface between fuel and ashes once burning has ceased.

effects, the variation in Table 1 is no big surprise and is illustrative of the uncertainty in our results. We emphasize though that this is not due to the numerical methods applied here, but due to the variable (and artificial) initial setup.

Viewed this way, the results of the resolution study can be understood in a straightforward manner. It should be noted that the resolution affects the answer in two ways. On the one hand, it affects the temperature in the collision because higher resolution smears out the hot spot less. But, on the other hand, it also affects the propagation of the flame as it moves outwards in the star, as illustrated by the variable explosion energy. Higher resolution decreases the discretization errors and therefore reduces the seeds for the growth of nonlinear perturbations. Therefore the flame develops less surface, less material is consumed and the lower energy release leads to a weaker expansion of the star. The material sweeping around at the surface is stronger gravitationally bound and the clash is more vigorous. Smaller initial flame bubbles are more sensitive to the numerical resolution. This is understandable since here bubble flotation is slower and nonlinear features invoked by discretization errors have more time to develop on the way to the surface of the WD.

An imaginary ideal situation with no discretization errors would suppress the nonlinear growth due to instabilities. But since the WD star is expected to be perturbed by pre-ignition convection and the flame is likely to ignite in multiple spots

TABLE 1
2D 200 km - 50 km . D

.

Model	bubble radius [km]	resolution	T_{max} at coll. [10^9 K]	E_{nuc} at coll. [10^{50} erg]	$T_{max}(\rho > 3{\times}10^6$ g cm^{-3}) at coll. [10^9 K]	$T_{max}(\rho > 1{\times}10^7$ g cm^{-3}) at coll. [10^9 K]	surface detonation?
2B50d200a	50	128×256	2.61	1.14	1.54	—	no
2B50d200b	50	192×384	2.92	0.97	2.60	—	yes
2B50d200c	50	256×512	2.22	1.46	1.28	—	no
2B50d200d	50	384×768	2.53	1.44	0.959	—	no
2B50d200e	50	512×1024	2.29	1.39	0.954	—	no
2B25d200a	25	128×256	2.40	1.33	2.08	—	no
2B25d200a	25	192×384	1.97	1.47	0.224	—	no
2B25d200a	25	256×512	2.60	1.09	2.32	—	yes
2B25d200a	25	384×768	3.03	0.72	3.03	2.95	yes
2B25d200a	25	512×1024	3.83	0.82	3.83	3.80	yes

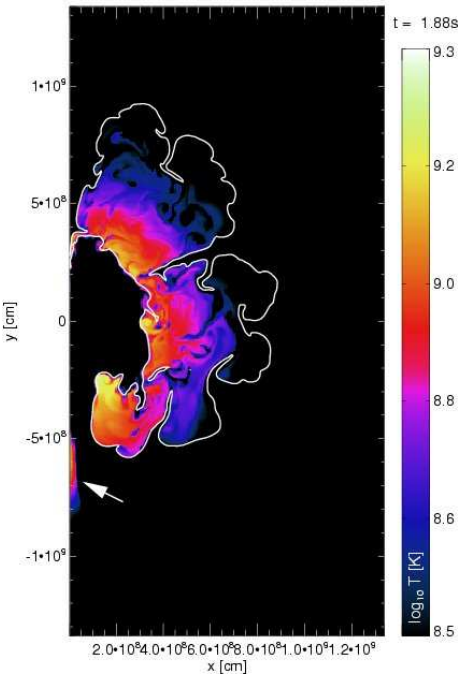

F . 2.— Temperature distribution Model 2B50d200c. The white contour indicates the zero-level set of G indicating the interface between fuel and ashes. Apart from the ash regions enclosed by this contour, significantly increased temperatures are found in the region compressed by the collision (marked by the white arrow).

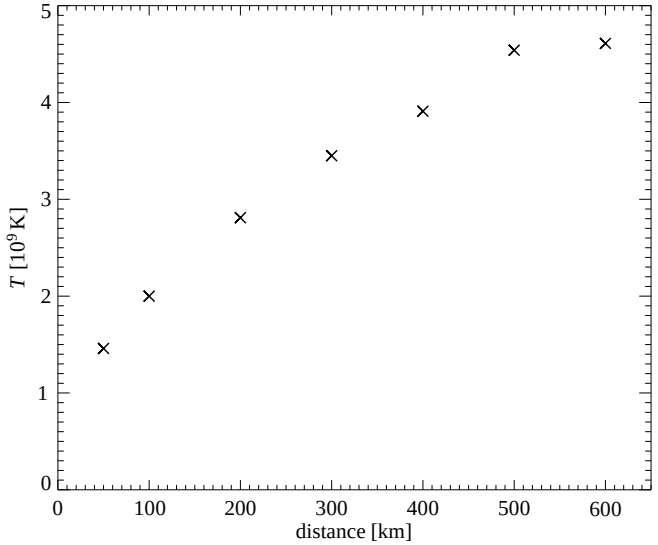

F . 3.— Maximum fuel temperature reached in the region of collision of the material sweeping around the WD as a function of the displacement of the initial flame bubble from the center of the WD (according to Table 2).

or an irregular shape, this seems far from reality.

Besides the energy release due to burning, the impact of the colliding material will also be sensitive to the morphology of the ash that is driving the unburned material like a piston. A well-defined, large leading edge of the colliding ash regions should result in a better focus than a multitude of leading features. Since the flame morphology is determined by nonlinear effects and instabilities, discretization errors in different resolutions amplify the scatter in the results.

4.1.2. *Bubble displacement*

The first physical parameter—the displacement of the initial flame bubble from the center—turned out to have substantial influence on the densities and temperatures reached in the collision. Values from simulations starting with an initial flame bubble of radius 25 km and varying distances from the center of the WD are given in Table 2. In order to minimize the scatter due to differences in resolution, the initial grid spacing of the 256×512 cells setup was held fixed for all simulations. Note, however, that since two nested grids are used to follow the expansion of the WD and the flame propagation, the resolution evolves according to the energy released in the burning, which is different in the various simulations. Nevertheless, a trend of increasing collision temperatures with larger initial flame displacements from the center of the WD is clearly visible (cf. Fig. 3). At large displacements the temperature increases less indicating a saturation of the effect. A possible explanation is that although here the expansion of the star prior to breakout is decreased, the amount of ashes expelled from the surface also decreases due to less burning taking place. Therefore the momentum of the colliding ash regions is smaller and the reduced impact leads to lower compression temperatures. Flames born closer to the center burn more material and cause more expansion (cf. Table 2). Displacing the initial flame bubble from 50 km to 600 km off-center decreases the nuclear energy release for 94% and increases the maximum temperature reached in the collision by 250%. Such a large displacement as 600 km is not realistic, but the consequences may be the same as for a bubble ignited closer in, but with a less efficient prescription for burning on the way out.

TABLE 2
C (2D ; : 25 km). D .

Model	distance from center [km]	$T_{\rm max}$ at coll. [10^9 K]	$E_{\rm nuc}$ at coll. [10^{50} erg]	$T_{\rm max}(\rho > 3{\times}10^6$ g cm^{-3}) at coll. [10^9 K]	$T_{\rm max}(\rho > 1{\times}10^7$ g cm^{-3}) at coll. [10^9 K]	surface detonation?
2B50d50	50	1.46	2.31	0.809	—	no
2B50d100	100	2.00	1.93	—	—	no
2B25d200	200	2.81	1.07	2.13	—	no
2B25d300	300	3.45	0.76	3.45	0.438	yes
2B25d400	400	3.91	0.46	3.91	3.91	yes
2B25d500	500	4.54	0.28	4.54	3.91	yes
2B25d600	600	4.61	0.12	4.61	4.61	yes

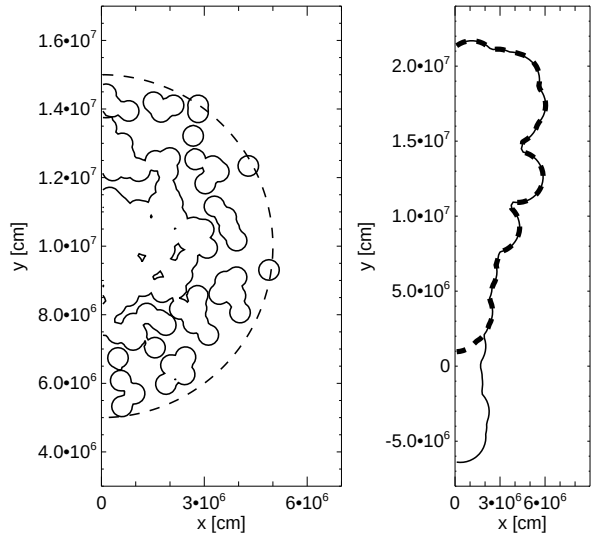

F . 4.— Different initial flame bubble morphologies. Left: perfect sphere (dashed) vs. irregular shape (solid); right: teardrop-shaped initial flames on one side of the WD's center (dashed) and overshooting to the opposite side of it (solid).

4.1.3. *Bubble morphology*

The initial morphology of the flame also affects the strength of the collision. Any divergence from a perfectly spherical shape has a similar effect to varying the resolution. In both cases, seeds for the developing instabilities are imposed—with changing resolution due to discretization errors, and for more complex initial bubble shapes, explicitly in a controlled way.

To demonstrate this, two simulations were carried out on a well resolved (384×768 cells) computational grid. One model (2B50d100, see Table 3) was ignited in a—within discretization error—perfectly spherical bubble of radius 50 km at a distance of 100 km from the center. In the second simulation (2P50d100), the initial flame was composed of 160 partially overlapping small bubbles of radius 3 km placed within a sphere of 50 km radius 100 km off-center of the WD (cf. Fig. 4, left).

While the spherical initial flame led to a maximum temperature of $4.25{\times}10^9$ K in the collision of the surface material and released 0.861×10^{50} erg prior to the collision, the irregular-shaped initial flame caused much more burning. It released 1.14×10^{50} erg before the clash, and the maximum temperature reached in the collision region was only 3.31×10^9 K (cf. Table 3).

4.1.4. *Irregular asymmetric ignition*

Due to the dipolar convection flow structure found in the pre-ignition phase by Kuhlen et al. (2006), a lop-sided flame ignition—possibly in many separate spots—is plausible. That ignition region may extend out to ∼200 km and reach down to the center of the WD. Some overshooting to the opposite side may also be possible if the actual flow is multipolar. The ignition kernels will quickly merge due to burning and the resulting flame structure may look like a teardrop with an irregular surface.

We examined two such configurations, one ignited on only one side of the WD (Model 2T1d100, cf. Table 3), and another in which the ignition extended through the center (Model 2T2d100). These ignition configurations are shown in the right hand plot of Fig. 4.

While the one-sided ignition evolution proceeded in a way similar to the single-bubble ignition simulations (Model 2B50d200c of Table 1 can serve as a reference simulation; its evolution is shown in Fig. 1), the extension of the ignition region to the opposite side of the WD's center had dramatic consequences. The burning did not ascend to the surface of the star on just one side, but evolved into two large irregular bubbles that moved in both directions (cf. Fig. 5). Naturally, the collision of material sweeping around the surface occurred off-axis. In this set-up, two opposing effects altered the collision strength. On the one hand, burning material on both sides of the star releases more energy and therefore the expansion of the star proceeds more rapidly. But, on the other hand, the collision occurs only slightly more than half way around the hemisphere, and therefore takes place earlier.

The reference Model 2B50d200c reached a collision temperature of 2.22×10^9 K at a density of 1.41×10^6 g cm^{-3} and released 1.46×10^{50} erg in the burning. The one-sided teardrop ignition led to similar values—a maximum temperature of 2.21×10^9 K at a density of 3.57×10^6 g cm^{-3} and a nuclear energy release of 1.25×10^{50} erg.

For the two-sided teardrop ignition, considerably more energy (2.30×10^{50} erg) was released in the burning prior to the collision. This decreased the collision strength dramatically. The temperature of the compressed fuel did not exceed 10^9 K (cf. Table 3), indicating that the effect of the earlier clash of the material coming from both poles cannot compensate for the enhanced expansion. However, it cannot be ruled out that multiple plumes breaking out at smaller angles with the center of the WD may collide more efficiently. But in this case the initial conditions have to be chosen carefully since bubbles too close to each other will merge before reaching the surface. Looking at the evolution of our models ignited in a single bubble, this seems rather hard to achieve. The snapshot at $t = 1.0$ s of Model 2B50d200c shown in fig. 1 indicates that by the time the burnt structure breaks our of the surface of the

C 2D . D

TABLE 3
.

Model	resolution	T_{max} at coll. [10^9 K]	E_{nuc} at coll. [10^{50} erg]	$T_{max}(\rho > 3{\times}10^6$ g cm$^{-3})$ at coll. [10^9 K]	$T_{max}(\rho > 1{\times}10^7$ g cm$^{-3})$ at coll. [10^9 K]	surface detonation?
2P50d100	384 × 768	2.31	1.14	2.31	0.507	yes
2B50d100	384 × 768	4.25	0.861	4.25	4.25	yes
2T1d200	256 × 512	2.21	1.25	0.991	—	no
2T2d200	256 × 512	0.958	2.30	0.0797	—	no

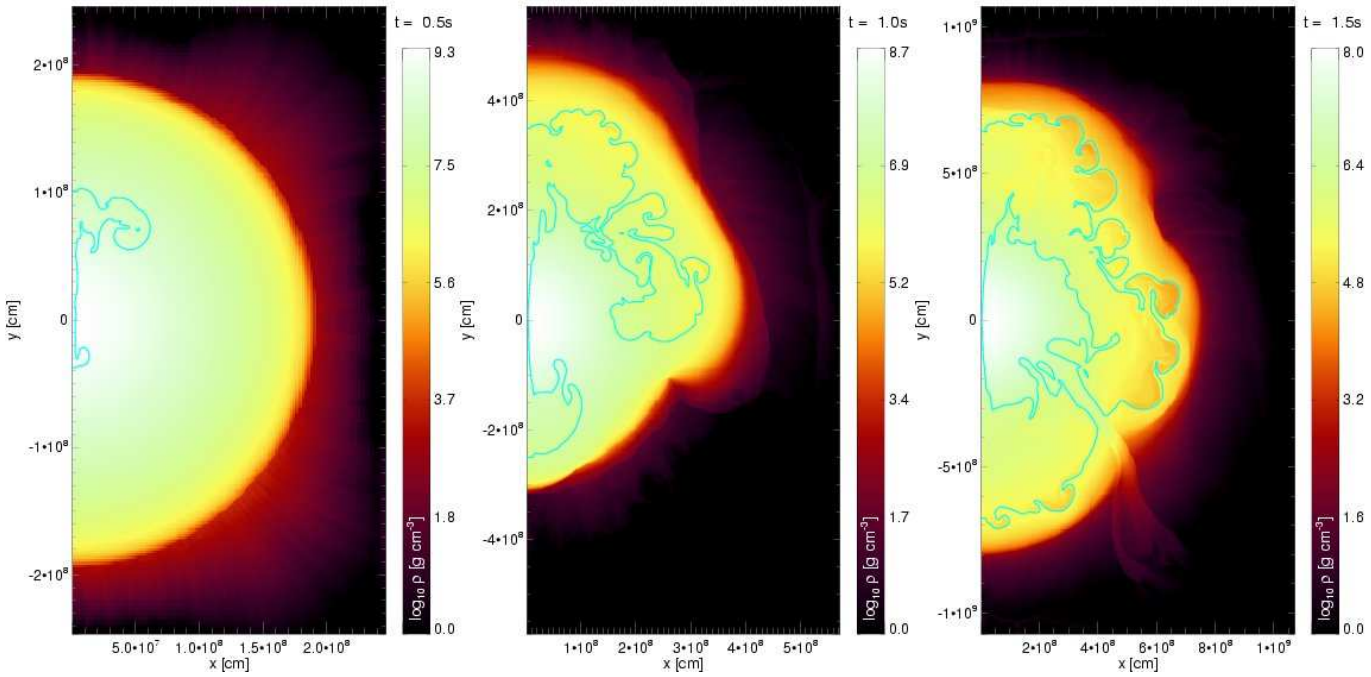

F . 5.— Evolution of an explosion simulation with the flame ignition extending to opposite sides of the WD (Model 2T2d200).

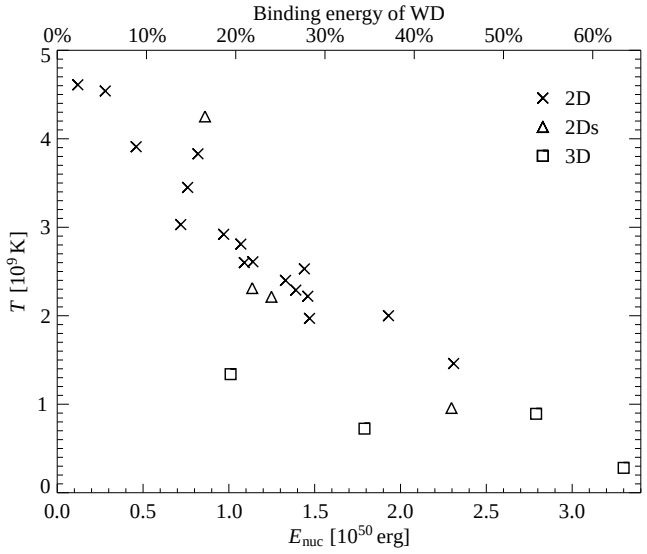

F . 6.— Maximum fuel temperature reached in the collision region as a function of the nuclear energy release prior to reaching that temperature according to Tables 1, 2 (data points marked "2D"), Table 3 (data points marked "2Ds") and Table 4 (data points marked "3D").

star, it spans an opening angle of about 180° with the WD's center making the opposite-sided ignition the best choice.

4.2. *Lessons learned from 2D simulations*

Our exploration of setup parameters in 2D simulations reveals that a key quantity determining the collision strength is the nuclear energy released on the flame bubble's way to the surface. Combining the data of Tables 1, 2, and 3, a clear correlation is visible between the maximum temperature reached in the collision of surface material and the amount of burning (cf. Fig. 6). Whether accomplished through a change in resolution, a displacement of ignition point, or a different morphology for the ignition region, less burning on the way out correlates with a stronger, hotter collision on the far side. This correlation arises naturally because the expansion of the star leads to the collision being spread out over a larger volume. The lower density also implies a greater heat capacity in the radiation field. On the other hand, more burning also implies more ash participating in the collision, which might make it stronger. But apparently the expansion effect dominates.

A potential concern is that insufficient resolution of the compressed fuel region might make the temperature measurements unreliable. However, the clear correlation shown in Fig. 6 originates from simulations with different resolutions. The data points lining up well is an indication that the temperature measurement was credible even in the less resolved simulations

The amount of fuel burned is a consequence of many uncertain aspects of the explosion physics, the specific algorithm

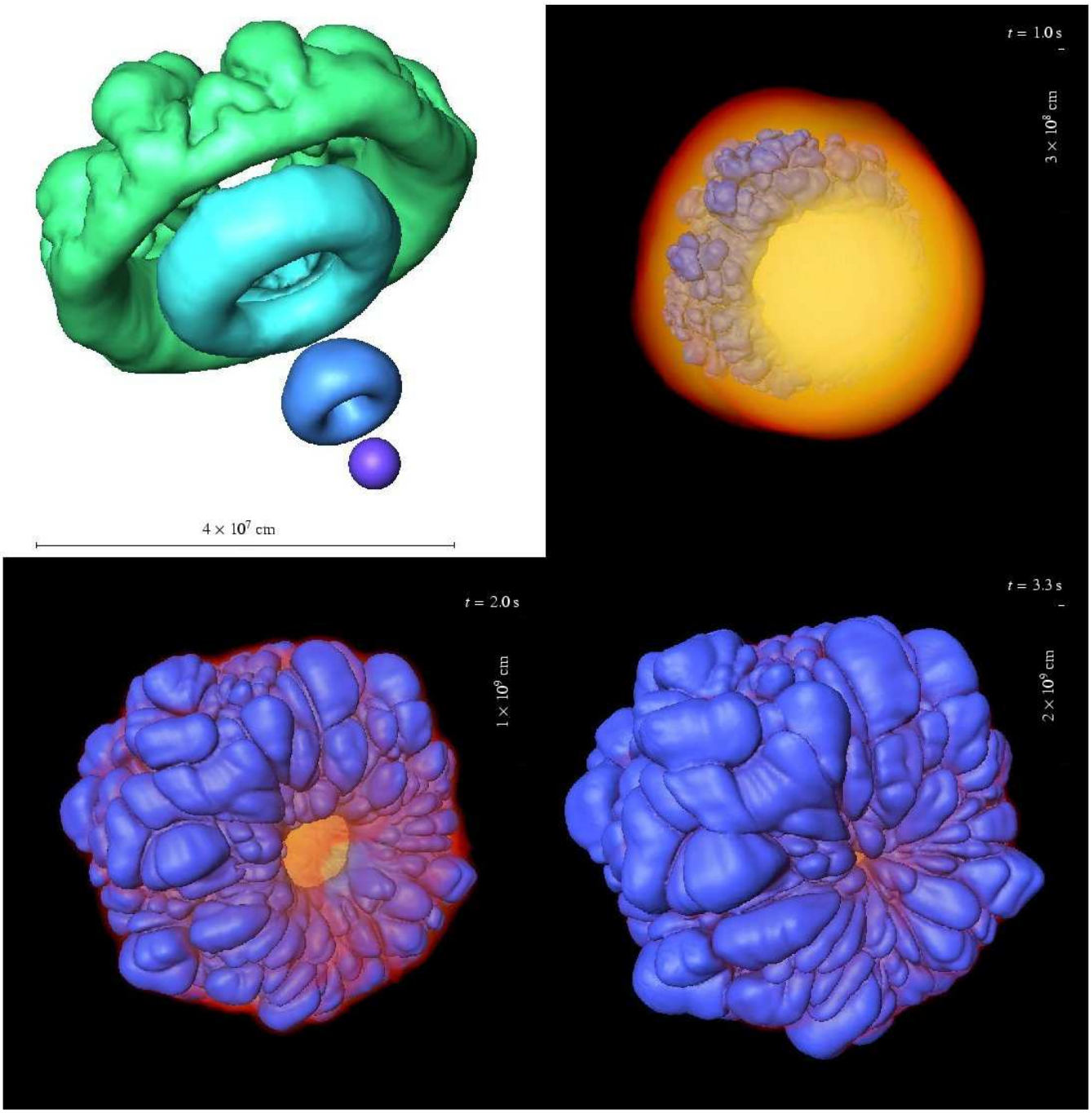

F . 7.— Evolution of a 3D explosion simulation with the flame ignition in a single bubble of radius 25 km displaced 100 km from the center of the WD (Model 3B25d100). Top left panel: initial evolution of the flame front (blue to green isosurfaces correspond to $t = [0, 0.25, 0.35, 0.45]$ s). Other panels: later evolution with the logarithm of the density volume rendered and $G = 0$ as blue isosurface indicating the flame front or, later, the approximate boundary between burned and unburned material.

used to implement the flame propagation, and the resolution of the simulation. For displacements that are not too extreme, stronger collisions are favored by increased distance of the ignition from the center. Alterations of the initial bubble shape diverging from the idealized spherical bubble model also have a substantial impact on the flame propagation. More complex initial flame shapes provide seeds for the developing nonlinear flame features.

Two-sided ignition naturally burns more material, leading to greater expansion. This is only partially compensated by the earlier collision time.

5. THE FULL STORY: 3D SIMULATIONS

The entire WD was mapped onto a *Cartesian* computational grid and, again, different ignition setups were tested. Compared with 2D, several general factors alter the collision strength in 3D. In the 2D-simulations, each flame feature corresponds to a torus extending around the star. Such complete burning does not occur in three dimensions, and so one might expect stronger collisions in 3D due to decreased expansion. On the other hand, the additional degree of freedom also enhances the growth of the flame surface due to instabilities. This effect has been seen in previous simulations where 3D-, centrally-ignited setups released significantly more en-

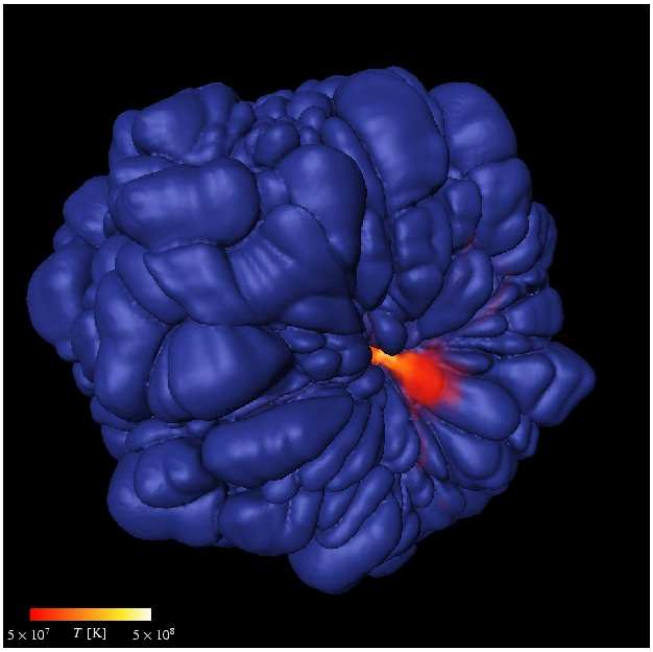

F . 8.— Snapshot of Model 3B25d100 at $t = 3.3$ s, as in Fig. 7, but here with the temperature volume rendered instead of the density.

ergy than their 2D-counterparts (Reinecke et al. 2002a; Röpke 2005). This causes more expansion and weaker collisions.

Finally, when the collision geometry is no longer restricted by cylindrical geometry, one expects less focusing, again weakening the collision strength.

5.1. *Single-bubble ignition*

In two of the simulations, the flame was again ignited as a single spherical bubble. The subsequent evolution is given in Fig. 7. Due to the interplay of burning and buoyancy, the burning bubble alters its shape from a sphere to a torus during the first few tenths of a second (cf., upper left panel of Fig. 7). This evolution is very similar to the results of Zingale et al. (2005) who simulated a burning bubble on small scales fully resolving the flame structure. The developing torus is more regular than the respective flame structures found in the 2D simulations. Nonetheless, it is subject to instabilities, and irregular features grow, mostly on the outward side of the burning region. The seeds for these features are probably discretization errors.

Once the ashes reach the outer parts of the star (n.b., not necessarily the surface), they start to sweep around its core. Interestingly, the leading edge of this sweeping material is defined, even in 3D, by the former torus and therefore only slightly irregular (cf. upper right and lower left panels of Fig. 7). Consequently, the clash of the burned material still takes place in a well-defined spot on the opposite side of the WD (cf. lower right panel of Fig. 7). In comparison with 2D simulations, this effect partially compensates for the lack of symmetry restrictions and makes the focus of the collision sharper than expected. In the collision, the temperature increases, as shown by the volume rendering of the temperature field in Fig. 8.

In the two simulations presented here, the initial flame bubbles were displaced 100 km (Model 3B25d100) and 200 km (Model 3B25d200) from the center of the WD, respectively. Both simulations were carried out on a $[512]^3$ cells computational grid. To gain the maximum possible resolution, the fine-spaced inner uniform part of the computational grid was extended only slightly beyond the ignition radius, and therefore the initial resolution of the flame was coarser in the model ignited further off-center. Contrary to the 2D study where the initial resolution was kept constant while varying the ignition position, we had to sacrifice comparability between the simulations to better resolution in the model ignited closer to the center. Because of the computational expense of 3D simulations, two parameters were changed at the same time, i.e., the distance of the ignition from the center and the perturbation imposed on the igniting bubble due to discretization errors.

TABLE 4
C 3D .

Model	$T_{\max}$ at coll. [10^9 K]	$E_{\rm nuc}$ at coll. [10^{50} erg]	ρ at coll. [10^6 g cm^{-3}]
3B25d100	0.892	2.79	$< 1.3 \times 10^5$
3P25d100	1.34	1.01	$< 1.5 \times 10^5$
3P50d100	0.724	1.79	$< 2.5 \times 10^5$
3B25d200	no collision: WD unbound		
3T1d200	0.281	3.30	$< 3.2 \times 10^3$
3T2d200	no collision: WD unbound		

Unlike the 2D results, the flame ignited at 200 km off-center released more energy in 3D than the one ignited at 100 km off-center. The reason, most likely, is the different discretization errors. The large features that develop at the end of the torus-dominated phase of the evolution were more pronounced in Model 3B25d200. Therefore more material was consumed and the energy release of 5.65×10^{50} erg was even sufficient to unbind the star (which has a binding energy of -5.20×10^{50} erg). In the simulation ignited 100 km off-center, the WD remained bound and the ashes breaking out of the surface swept around the core and collided on the opposite side as illustrated in Fig. 7.

To gain more control over the initial perturbations that later affect the growth and buoyancy of the flame, two additional simulations were carried out where the ignition was, on the average, spherical, but actually composed of many smaller spheres of hot ash, so that the seeds for instabilities were present from the beginning. One, Model 3P25d100, had parameters similar to Model 3B25d100, with the center of the ignition region positioned 100 km off-center, and the small flame kernels located inside a radius of 25 km. For the second, Model 3P50d100, the displacement of the center of the flame was unchanged, but the spherical aggregate of small bubbles filled a larger volume with radius of 50 km. In contrast to the 2D simulation, the perturbations applied here decreased the amount of burning (Table 4). This can be understood from the the temporal evolution of the energy release and the bubble morphology. In the beginning, the energy release in the highly perturbed case exceeds that for a smooth sphere, as expected from the faster development of its flame surface. However, this irregularity prevents the perturbed bubble from evolving a stable, toroidal structure. In terms of the overall energy release, the toroidal shape seems to be a favorable configuration. For the spherical bubble models, as soon as irregular features form on top of the torus, the energy release increases dramatically. This boost in the burning rate is much weaker for the perturbed case.

In our 3D simulations, nuclear burning was suppressed three seconds after ignition. In all models but 3P50d100, it actually ceased earlier, since the fuel density in front of the flame fell below the threshold for burning, 10^7 g cm^{-3}. For

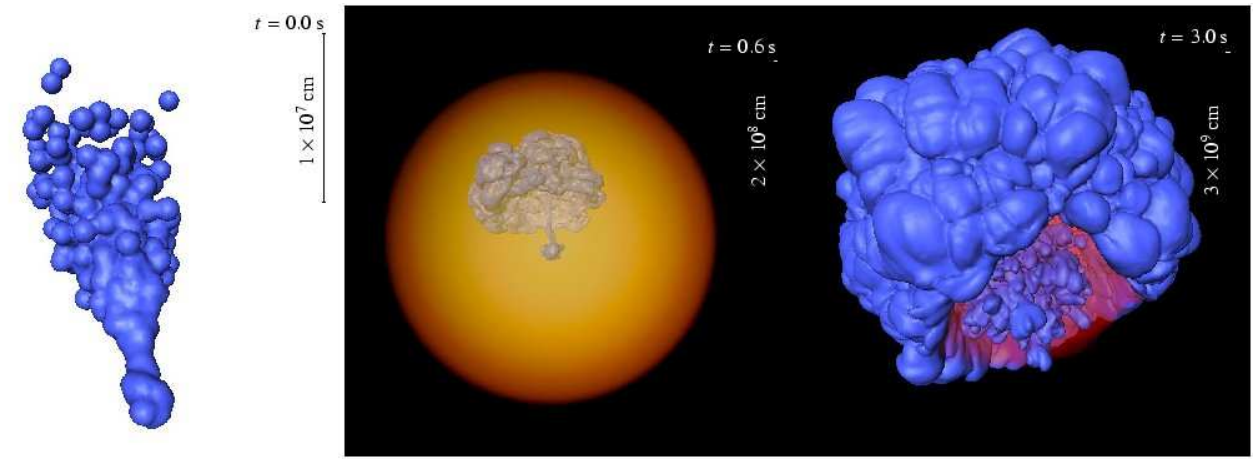

F . 9.— Evolution of an explosion simulation with the flame ignition in a two-sided teardrop shape (Model 3T2d200). The first snapshot shows the initial flame (blue isosurface) with parts extending to both sides of the center of the WD. This leads to a two-sided evolution of the flame inside the WD, whose extend is indicated by the volume rendering of the logarithm of the density (center panel). The energy released in the thermonuclear burning is sufficient to overcome the gravitational binding of the star, giving rise to a weak explosion. In the right snapshot, the blue isosurface now indicates the approximate interface between burned and unburned material. This configuration is approaching homologous expansion and no collision between ash regions will take place at the surface of the star.

Model 3P50d100, however, burning was still active at $t = 3$ s. Therefore, the nuclear energy release is only a lower limit for this calculation, and the maximum temperature in the collision (found at $t = 4.81$ s) is an upper bound.

5.2. *Irregular asymmetric and dipolar ignitions*

As in the 2D simulations, irregular one- and two-sided teardrop-shaped initial flame setups were employed. The evolution of the two-sided flame ignition case (Model 3T2d200) is shown in Fig. 9. Once more, the flame propagates in two opposite directions. Unlike the 2D simulations, however, the burning releasing 8.16×10^{50} erg is sufficient and unbind the star. The shape shown in the right panel of Fig. 9 marks the final stage of the evolution approaching homologous expansion. No strong collision of surface material occurred.

Model 3T1d200, initiated with a one-sided teardrop-shaped flame, released about two-thirds of the WD's binding energy. As with the other bubble ignitions, the burning material floated towards the surface, swept around the core of the WD, and clashed on the opposite side. The collision parameters are listed in Table 4.

5.3. *Summary of the 3D simulations*

The diversity of results found in 3D simulations is larger than that in 2D simulations. The measured quantities are summarized in Table 4. In two of the models the WD was even unbound. As plotted in Fig. 6, all peak collision temperatures in 3D simulations were lower than those in 2D.

A direct comparison between 2D and 3D models is difficult since models with similar initial flames (in spherical or teardrop-like shapes) release significantly more energy when performed in 3D. The only way we found to lower the energy release here was by explicitly perturbing the initial bubble. The two corresponding models, 3P25d100 and 3P50d100, releasing 1.01×10^{50} erg and 1.79×10^{50} erg of energy in burning, can be compared to 2D simulations releasing similar amounts of nuclear energy. The closest examples would be 2B50d200b (0.97×10^{50} erg) and 2B50d100 (1.93×10^{50} erg). These achieved collision temperatures of 2.92×10^9 K and 2.00×10^9 K, respectively, while the collision temperatures for the 3D models were significantly lower (1.34×10^9 K and 0.724×10^9 K).

TABLE 5
C .

ρ [10^6 g cm^{-3}]	T_c [10^9 K]	M [g]	R [km]	detonation?
10	2.6	2.5×10^{23}	2	no
10	2.7	2.5×10^{23}	2	no
10	2.8	2.5×10^{23}	2	yes
10	2.1	2.0×10^{25}	8	no
10	2.2	2.0×10^{25}	8	yes
10	1.8	1.5×10^{27}	30	no
10	1.9	1.5×10^{27}	30	yes
3	2.2	2.0×10^{28}	120	no
3	2.3	2.0×10^{28}	120	yes
1	2.4	3.0×10^{27}	90	no
1	3.0	3.0×10^{27}	90	no
1	3.0	3.0×10^{30}	900	no

Two interpretations are possible here. Either the collision temperatures are generally lower in 3D due to the additional degree of freedom decreasing the focusing, or this may only be the case for models started with strong perturbations from a spherical bubble since here the toroidal structure supporting focusing is suppressed. In the first case, the relation between collision temperature and energy release would be swallower for the 3D data points in Fig. 6 than the relation for the 2D data points. In the second case, the two 3D data points for the highest energy releases would fall onto the relation for the 2D sample and the two low-energy 3D models would diverge from it.

6. CONDITIONS FOR DETONATION

6.1. *Constraints on detonation ignitions in degenerate C+O matter*

In order to trigger a detonation a region must burn supersonically and the size of that region must be larger than some critical mass (Niemeyer & Woosley 1997; Dursi & Timmes 2006). Because that critical mass is very sensitive to the density and composition, detonation becomes increasingly difficult at low density and is sensitive to the carbon mass fraction in the unburned fuel.

A series of calculations was carried out offline to study the

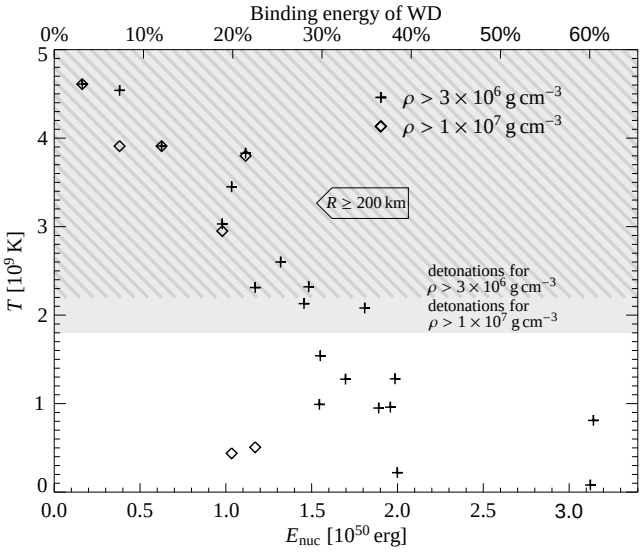

F . 10.— Maximum temperature reached in the collision region for fuel above the given density thresholds as a function of the nuclear energy release prior to reaching the maximum collision temperature (according to Tables 1, 2 and 3). The shaded and dashed regions correspond to conditions where an initiation of a detonation is possible for temperatures reached in fuel of densities $\rho > 1\times10^7$ g cm^{-3} and $\rho > 3\times10^6$ g cm^{-3}, respectively.

conditions for detonation using the K 1D hydrodynamics code (Weaver et al. 1978). The procedure was identical to that described in Niemeyer & Woosley (1997).

A sphere composed of 50% by mass carbon and 50% oxygen of prescribed density, ρ, was given a temperature profile characterized by a central value, $T_{\rm c}$, and a linear decline over a specified range of mass, M, defining a radius, R, of the sphere. The sphere was then allowed to runaway inside of a much larger, cooler isothermal region to see if a successful detonation resulted.

Table 5 gives the results. If the compression heats fuel with density above 10^7 g cm^{-3} to a temperature over 1.9×10^9 K on a length scale of 10 km or more (the grid resolution) detonation will occur. By 3×10^6 g cm^{-3}, the necessary temperature has risen to about 2.3×10^9 K on a scale of 100 km, and by $\rho = 1\times10^6$, *it is impossible to detonate the star no matter what temperature is achieved in the collision*. The critical mass has become more than a substantial fraction of the entire star. Even though burning might occur with a supersonic phase velocity, detonation of carbon does not happen below 10^6 g cm^{-3}.

6.2. *Comparison with simulations*

Since it is the combination of temperature and density reached in a critical mass that decides whether detonation occurs, the maximum temperatures in the collision region were measured in our 2D simulations at a density exceeding 1×10^7 g cm^{-3} and 3×10^6 g cm^{-3}, respectively. Values are given in Tables 1, 2, and 3, and the results are plotted in Fig. 10. Densities in the compressed material above 10×10^7 g cm^{-3} are only found in some rare cases in which the nuclear energy release prior to collision was lower than 1.2×10^{50} erg. For all simulations with an energy release lower than 2×10^{50} erg, the compression density of the unburned material in the collision exceeded $\sim3\times10^6$ g cm^{-3} and the temperature was determined there.

From these measurements, we find that *a detonation is admissible in some of the 2D models*. In models with single-bubble ignitions displaced more than 200 km off-center, sufficient temperatures are reached at densities exceeding the threshold of 3×10^6 g cm^{-3}. The spatial extent of the compressed region is not critical, since it is, at most, several grid cells in all cases (typical cell sizes in the collision region are several km). In models ignited at distances $\geq$ 400 km off-center, temperatures above 2.5×10^9 K were reached even at densities above 10^7 g cm^{-3}, rendering a detonation virtually certain. A bubble displacement around 200 km marks the bifurcation value, where secondary parameters, such as resolution, determine the feasibility of a detonation (cf. Table 1). It seems unlikely that the flame ignition takes place at such large radii in SNe Ia, but similar results might come from a model with less efficient lateral burning ignited closer in.

In all 3D simulations, the maximum compression temperatures in the collision (if one occurs at all) are too low to initiate a detonation. Moreover, these peak temperatures were found in material of densities falling short of the detonation threshold for at least one order of magnitude (cf. Table 4). The compressed region did not reach densities above 10^6 g cm^{-3} near temperature maximum in any of the simulations, the reasons thereof being the same as those discussed in Sect. 5.3. Even the 3D simulations releasing similar amounts of energy as some 2D simulations favoring a detonation did not reach the necessary densities. In the two-sided ignition Model 3T2d200 the the effect of an increased energy release was even greater than its the 2D analog—it unbound the star. Thus, all 3D simulations clearly fail to trigger a detonation.

7. CONCLUSIONS

The evolution of thermonuclear supernova models that ignite asymmetrically has been followed in two and three dimensions. Parameters of the setup, such as the numerical resolution, the displacement of the center of flame ignition from the center of the WD, and the ignition shape were explored in a systematic way in 2D, and the more interesting cases were explored in 3D.

For all 2D simulations, the energy release in the nuclear burning falls short of unbinding the star. In the cases with one-sided ignition, the flame floats rapidly to the surface (see also, Livne et al. 2005), spreading laterally as it goes due to burning and instabilities. Since the star is still gravitationally bound, the emerging ashes sweep around the core of the WD and collide on the opposite side, in agreement with Plewa et al. (2004). The collision strength, and thus the maximum temperature reached in the compressed fuel correlate inversely with the nuclear energy released on the flame's way to the surface. The question of whether the compression of unburned material in the collision region is adequate to trigger a detonation was explored in detail, and the necessary criteria were set out. A detonation can only occur if the fuel temperature exceeds approximately 1.9×10^9 K at a density above 10^7 g cm^{-3}. At lower densities, detonation requires higher temperatures and eventually becomes impossible, for any temperature, for densities less than about 10^6 g cm^{-3}.

The conditions for initiating a detonation were met in several 2D calculations in which the flame ignited in a spherical bubble more than 200 km off-center. Less efficient prescriptions for the burning might have found similar conditions in simulations that ignited closer in. For the initial conditions and flame propagation model assumed, the results of Plewa et al. (2004), may be reasonable. However, since the flame model applied there is not based on a consistent treatment of the flame's interaction with the turbulent cascade, it is difficult to judge its validity.

In three dimensions, all simulations fell far short of initiating a detonation. Some even released sufficient energy to unbind the star. There are several reasons for this difference. Lacking the artificial symmetry of 2D simulations, the focusing of the collision in 3D models can be weaker. Indications for this were found in our simulations. At least two of the 3D simulations gave significantly lower collision temperatures than predicted by 2D models that burned similar amounts of fuel (see Fig. 6). A second, probably dominant effect is that 3D models release more energy than their 2D analogs. This is mostly due to the additional degree of freedom in developing flame surface area due to instabilities. Another contribution to the difference may be the improved subgrid-scale turbulence model applied in the 3D simulations. However, this effect is expected to be minor (Schmidt et al. 2006b). An asymmetrically ignited 3D model based on a different flame implementation (Calder et al. 2004) burned $\sim 0.075\,M_\odot$ of material. This corresponds to a nuclear energy release of $\sim 1.2\times 10^{50}$ erg—a value that falls in the range spanned by our parameter study. Therefore, although the Calder et al. model was not followed beyond the breakout of the ashes from the surface, one expects that that model would also have failed to trigger a detonation.

While we found no example of a successful detonation in our 3D simulations, this possibility cannot be completely ruled out since the exploration of the parameter space was incomplete. An interesting possibility is that of double-sided ignitions, which may be possible in a teardrop-shaped ignition overshooting through the WD's center (or, in a simpler configuration, as two opposed bubbles). Such a configuration shortens the way the material has to travel towards the collision spot once ashes break out of the star's surface on both sides. Therefore the expansion of the star may not be as advanced as in the collision on the far side of a single-bubble breakout. In this case, higher temperatures and densities are expected in the compressed fuel. On the other hand, burning on both sides of the star releases more energy while the flames propagate towards the surface. This increases the expansion prior to collision. In our simulations, the latter effect dominated and the collision was weak in a 2D model. A similar 3D model became unbound and no detonation was found in either. Thus, if a multiple surface breakout scenario is to work at all, no more than two widely separated ignition kernels are admissible or there will be too much expansion. An open question is whether a special placement of two or three bubbles spanning a smaller angle than 180° with the WD's center might favor the first effect, increasing the collision strength by shortening the path of the surface material. However, the bubbles cannot be too close or they would merge quickly due to burning, without significantly compressing the unburned material between them, and there cannot be very many, or they will prematurely unbind the star.

Keeping in mind the uncertainties of the flame model and the incompleteness of the parameter space explored in 3D simulations, we conclude, that although a detonation due to the colliding surface material may, in principle, occur for certain—possibly artificial—ignition configurations, it cannot serve as a robust model for SNe Ia. The simulations presented here indicate that it may not be realized in nature at all.

For models that remain gravitationally bound, failure to initiate a detonation will lead to pulsations of the WD star (Nomoto et al. 1976). This may be a second chance for triggering a detonation (Arnett & Livne 1994; Bravo & García-Senz 2006) and this occurrence will be addressed in a follow-up study.

This research used resources of the National Center for Computational Sciences at Oak Ridge National Laboratory, which is supported by the Office of Science of the U.S. Department of Energy under Contract No. DE-AC05-00OR22725. The work was supported by the NASA theory program (NNG05GG08G)and the SciDAC Program of the DOE (DE-FC02-01ER41176).

REFERENCES

Arnett, D., & Livne, E. 1994, ApJ, 427, 315
Blinnikov, S. I., Röpke, F. K., Sorokina, E. I., Gieseler, M., Reinecke, M., Travaglio, C., Hillebrandt, W., & Stritzinger, M. 2006, A&A, 453, 229
Bravo, E., & García-Senz, D. 2006, ApJ, 642, L157
Calder, A. C., Plewa, T., Vladimirova, N., Lamb, D. Q., & Truran, J. W. 2004, astro-ph/0405126
Colella, P., & Woodward, P. R. 1984, J. Comp. Phys., 54, 174
Damköhler, G. 1940, Z. f. Elektroch., 46, 601
Dursi, L. J., & Timmes, F. X. 2006, ApJ, 641, 1071
Filippenko, A. V. 1997, ARA&A, 35, 309
Fryxell, B. A., Müller, E., & Arnett, W. D. 1989, Hydrodynamics and nuclear burning, MPA Green Report 449, Max-Planck-Institut für Astrophysik, Garching
Gamezo, V. N., Khokhlov, A. M., Oran, E. S., Chtchelkanova, A. Y., & Rosenberg, R. O. 2003, Science, 299, 77
García-Senz, D., & Bravo, E. 2005, A&A, 430, 585
Garcia-Senz, D., & Woosley, S. E. 1995, ApJ, 454, 895
Hillebrandt, W., & Niemeyer, J. C. 2000, ARA&A, 38, 191
Höflich, P., & Stein, J. 2002, ApJ, 568, 779
Iapichino, L., Brüggen, M., Hillebrandt, W., & Niemeyer, J. C. 2006, A&A, 450, 655
Khokhlov, A. M. 1991, A&A, 245, 114
Kozma, C., Fransson, C., Hillebrandt, W., Travaglio, C., Sollerman, J., Reinecke, M., Röpke, F. K., & Spyromilio, J. 2005, A&A, 437, 983
Kuhlen, M., Woosley, S. E., & Glatzmaier, G. A. 2006, ApJ, 640, 407
Livne, E., Asida, S. M., & Höflich, P. 2005, ApJ, 632, 443
Niemeyer, J. C. 1999, ApJ, 523, L57
Niemeyer, J. C., & Hillebrandt, W. 1995, ApJ, 452, 769
Niemeyer, J. C., Hillebrandt, W., & Woosley, S. E. 1996, ApJ, 471, 903
Niemeyer, J. C., & Woosley, S. E. 1997, ApJ, 475, 740
Nomoto, K., Sugimoto, D., & Neo, S. 1976, Ap&SS, 39, L37
Osher, S., & Sethian, J. A. 1988, J. Comp. Phys., 79, 12
Plewa, T., Calder, A. C., & Lamb, D. Q. 2004, ApJ, 612, L37
Pocheau, A. 1994, Phys. Rev. E, 49, 1109
Reinecke, M., Hillebrandt, W., & Niemeyer, J. C. 2002a, A&A, 386, 936
—. 2002b, A&A, 391, 1167
Reinecke, M., Hillebrandt, W., Niemeyer, J. C., Klein, R., & Gröbl, A. 1999, A&A, 347, 724
Röpke, F. K. 2005, A&A, 432, 969
Röpke, F. K., Gieseler, M., Reinecke, M., Travaglio, C., & Hillebrandt, W. 2006a, A&A, 453, 203
Röpke, F. K., & Hillebrandt, W. 2004, A&A, 420, L1
—. 2005a, A&A, 431, 635
—. 2005b, A&A, 429, L29
Röpke, F. K., Hillebrandt, W., Niemeyer, J. C., & Woosley, S. E. 2006b, A&A, 448, 1
Schmidt, W., & Niemeyer, J. C. 2006, A&A, 446, 627
Schmidt, W., Niemeyer, J. C., & Hillebrandt, W. 2006a, A&A, 450, 265
Schmidt, W., Niemeyer, J. C., Hillebrandt, W., & Röpke, F. K. 2006b, A&A, 450, 283
Travaglio, C., Hillebrandt, W., Reinecke, M., & Thielemann, F.-K. 2004, A&A, 425, 1029
Weaver, T. A., Zimmerman, G. B., & Woosley, S. E. 1978, ApJ, 225, 1021
Woosley, S. E. 1990, in Supernovae, ed. A. G. Petschek (New York: Springer-Verlag), 182–212
Woosley, S. E., & Weaver, T. A. 1994, in Les Houches Session LIV: Supernovae, ed. S. Bludman, R. Mochovitch, & J. Zinn-Justin (Amsterdam: North-Holland), 63–154
Woosley, S. E., Wunsch, S., & Kuhlen, M. 2004, ApJ, 607, 921
Wunsch, S., & Woosley, S. E. 2004, ApJ, 616, 1102

Zingale, M., Woosley, S. E., Bell, J. B., Day, M. S., & Rendleman, C. A.
2005, Journal of Physics Conference Series, 16, 405